ADVANCED FUNCTIONAL MATERIALS
www.afm-journal.de

Empty-State Band Mapping Using Momentum-Resolved Secondary Electron Emission

*Gary Wan, Alex Croot, Neil A. Fox, and Mattia Cattelan**

Material band structures of occupied electronic states are obtainable using conventional angle-resolved photoemission experiments, leaving the unoccupied states far less explored. Here, an alternative approach is built on and expanded to investigate thermalized photoelectrons emitted from crystal surfaces. A model for electron emission is constructed and reveals the material unoccupied state band structure. Potentially applicable to any material and independent from the secondary electron generation mechanism, it is demonstrated on diamond and copper using different light sources. Moreover, the diamond indirect band gap is directly observed and the transverse effective mass at the conduction band minimum can be experimentally obtained, $m_t = (0.21 \pm 0.015)\ m_e$. This offers a convenient path for angle-resolved photoemission data interpretation and empty-state information extraction.

1. Introduction

Unoccupied band structure provides valuable information on electron–phonon dynamics,[1–3] excitons,[4] superconductivity,[3,5] band gap estimation,[2] molecular adsorption,[6] and surface states.[7] Understanding the directional and energetic behavior of carriers in unoccupied states is also key to optimizing devices such as transistors,[8] optoelectronics,[9] valleytronics,[10] spintronics,[11] and thermionics.[12]

A few techniques have been developed to study unoccupied states including inverse photoemission spectroscopy,[6] scanning tunneling spectroscopy,[13] and low energy electron emission.[14,15] While these techniques have demonstrated the ability to acquire information about empty states, they have been largely overlooked in the recent years, likely due to the difficulty in data interpretation and complexity of experiments. On the other hand, time-resolved spectroscopy[16] and its application in time-resolved angle-resolved photoemission spectroscopy (ARPES),[2,17] are still extensively studied. The latter is one of the more advanced techniques and can resolve momentum, energy, and lifetime of electrons in excited states. However, pump–probe ARPES experiments are similarly complex and further limited by space-charging effects.[2,18]

Here we show a method to directly observe the unoccupied electronic band structure of crystals, using a new interpretation of the low kinetic energy region of photoemission spectra. This region is typically regarded as a secondary electron background containing little structural information.[19] A relatively simple ARPES apparatus using conventional laboratory-based continuous wave light sources is used to obtain important empty-state information. ARPES utilizes the photoelectric effect and momentum conservation to examine the band structures of crystals, providing a powerful tool typically used to observe occupied electronic states. Photoelectrons are emitted with their energy and surface-parallel crystal momentum $\hbar k_\parallel$ is conserved[20] and thus the energy–momentum dispersion relation, that is, band structure, can be mapped. On the other hand, non-emitted photoexcited electrons can relax to previously unoccupied states before being emitted, which may also provide useful information, provided that the emission process is well understood. For electron emission to occur, the energy and $k_\parallel$ must lie within a parabola defined by the free-electron dispersion relation,[21]

$$E = \frac{\hbar^2 k_{\parallel,max}^2}{2m_e} + V \tag{1}$$

where E is the energy level, $k_{\parallel,max}$ is the maximum parallel wavenumber, m_e is the electron mass and V is the potential at the electron position (i.e., 0 in vacuum and the inner potential when in a material).

The observation of empty-state features in photoemission has been noted in the past,[22,23] where the unoccupied density of states was found to correlate to peaks in the emission spectra.

G. Wan, Dr. N. A. Fox
Bristol Centre for Functional Nanomaterials
University of Bristol
Tyndall Avenue, Bristol BS8 1TL, UK
G. Wan, Dr. A. Croot, Dr. N. A. Fox
School of Physics
HH Wills Physics Laboratory
University of Bristol
Tyndall Avenue, Bristol BS8 1TL, UK
Dr. N. A. Fox, Dr. M. Cattelan
School of Chemistry
University of Bristol
Cantocks Close, Bristol BS8 1TS, UK
E-mail: mattia.cattelan@elettra.eu
Dr. M. Cattelan
Elettra-Sincrotrone Trieste ScPA
Strada Statale 14 - km 163,5 in AREA Science Park, Trieste 34149, Italy
The ORCID identification number(s) for the author(s) of this article can be found under https://doi.org/10.1002/adfm.202007319.

DOI: 10.1002/adfm.202007319

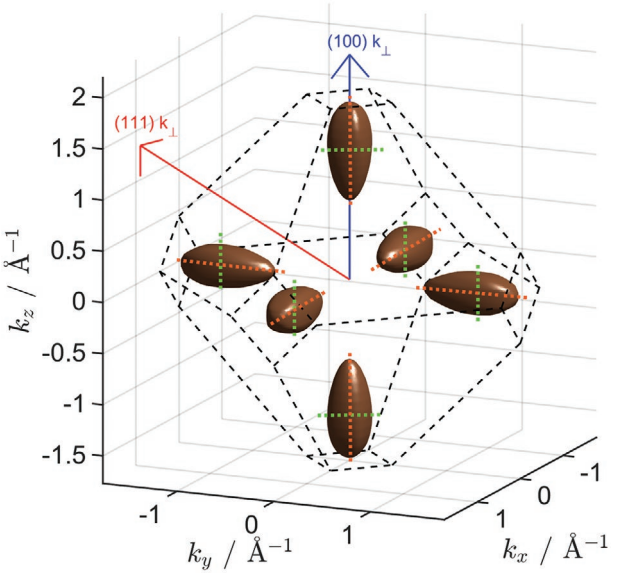

Figure 1. Energy isosurface of calculated bulk diamond bands at 6 eV above the VBM (0.5 eV above the CBM). The electronic states are shown in brown in 3D k-space, where the six valleys do not exist at $k = 0$, showing the indirect band gap of diamond. The axes are along the <100 > direction in k-space, while the blue and red arrows represent the $k_\perp$ viewing direction for the (100) and (111) surfaces, respectively. The transverse and longitudinal directions of each valley are also indicated by the green and orange dashed lines.

Bovet et al. showed that structure originating from empty states can be observed with angle-resolved spectra,[24] analogous to results from very low energy electron diffraction.[15] In this article, we present full-wavevector ARPES data with theoretical bands to investigate the emission rules and mechanisms from these states, which is directly compared with the well-established conventional ARPES.

2. Results and Discussion

Diamond is a wide band gap semiconductor that exhibits a large negative electron affinity (NEA) of about 1 eV when hydrogen terminated,[25,26] meaning the vacuum level lies below the conduction band minimum (CBM), allowing a significant proportion of electrons in the CBM to be emitted, according to Equation (1). Diamond also has a Si-like indirect band gap where the CBM lies along the six <100 > directions at 0.76 times the distance from Γ–*X*,[27] as depicted in **Figure 1**.

The calculated bulk diamond band structure at a single energy near the CBM is represented in 3D k-space in Figure 1, showing a single Brillouin zone. The indirect band gap is observed from the lack of states at (k) = 0 (Γ). The six valleys elongate with increasing energy and meet at Γ to form a larger direct energy gap with the valence band maximum (VBM) (Movie S1a, Supporting Information). Conventional ARPES without a tunable light source generally samples only a single 2D cut of the occupied band structure,[20,21] while the unoccupied electronic states are inaccessible. However, due to the NEA of diamond, any electrons thermalized from a higher energy state into the conduction band can also be emitted barrier free into the vacuum as secondary electrons. This has been observed frequently in the past in the form of a NEA peak in UV photoelectron spectroscopy (UPS).[25,28–30]

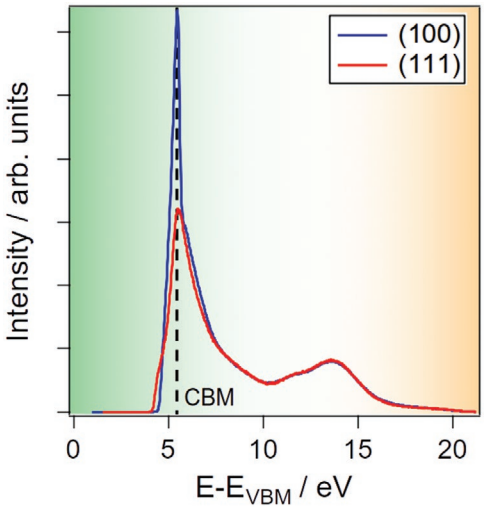

Figure 2. Full-wavevector UPS spectra of the hydrogen terminated (100) (blue) and (111) (red) diamond, $h\nu = 21.2$ eV. The x-axis is energy relative to the VBM position (E_{VBM}). The lower and higher energy regions are dominated by the conduction band and valence band structures, respectively. The CBM position is indicated by the black line.

The UPS spectra from two diamond orientations are shown in **Figure 2**, where a high intensity peak is observed near the CBM. The lower energy region indicated by green is dominated by the band structure of the initially unoccupied states, which are populated only after photoexcitation and relaxation by secondary electrons. Meanwhile, the yellow region predominately reflects the occupied valence band structure where ARPES measurements are typically carried out.[21] The high intensity peak position approximately corresponds to the energy position of Figure 1, where the electron density in the conduction band is highest. The secondary electron tail extends up to around 10 eV, decreasing exponentially in intensity. This is expected from the thermalization of excited electrons in the conduction band, following the Maxwell–Boltzmann distribution.[31] The intensity at the lower energies extends to over 1 eV below the CBM before reaching zero at the vacuum energy level. The electron emission below the CBM originates from within the band gap, which has been attributed to surface emissions,[14] and is discussed further below.

The higher energy region of Figure 2 consists of elastically scattered electrons which were photoexcited from the initially occupied valence band states, which have their initial wavevector conserved with an energy shifted up by the incoming photon energy, $h\nu$. Conventional ARPES is typically performed in this energy region, close to the VBM; it has well-defined momentum and energy conservation rules providing precise valence band dispersion information. At the lower energies, the inelastic scattering of electrons makes the emission more complex and is therefore generally considered significantly less useful.

Performing ARPES measurements within the green region in Figure 2 allows better understanding of the electronic states from which the electrons originate after thermalization and is compared side-by-side with our theoretical models. **Figure 3** shows the electronic states at 1 eV above the CBM, where on

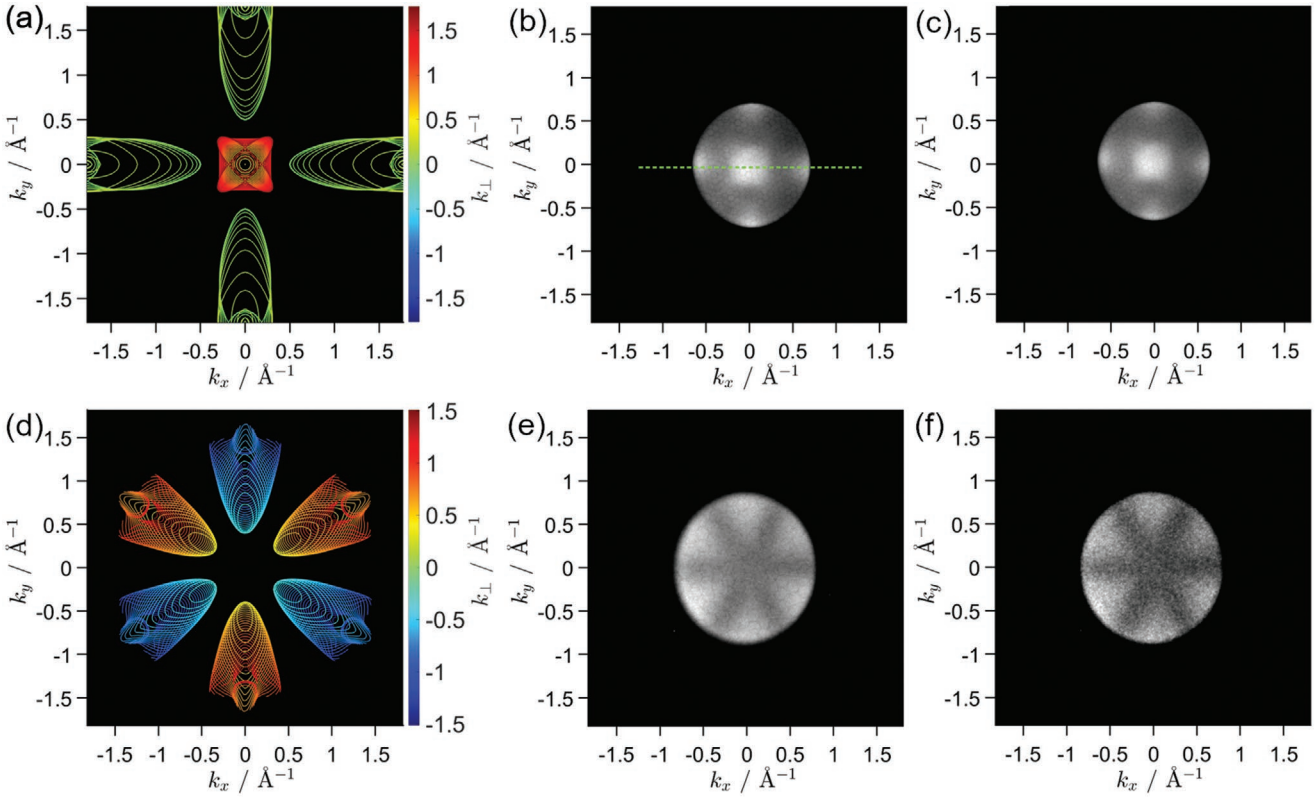

Figure 3. a,d) Modeled ARPES images using calculated bulk band structure compared with experimental full-wavevector ARPES images using b,e) 21.2 eV and c,f) 40.8 eV photons. The crystal orientations are (a,b,c) (100) and (d,e,f) (111). The energy is at 6.5 eV above the VBM. (a,d) Each calculated band is colored to represent its initial position along $k_\perp$ in the bulk (Figure 1) relative to Γ, which were taken through the Brillouin zone at intervals of 0.035 Å^{-1}. The dashed green line in (b) indicates the direction $X - \Gamma - X$.

the experimental images, more than a single feature is observed due to the six CBM valleys from the indirect band gap of diamond.[10,27] Five of the six valleys appear for the (100) surface, and all six on the (111). This is due to two of the valleys overlapping at $k_\parallel = 0$ on the (100) surface, illustrated by Figure 1 when viewing along the blue (100) arrow. The calculated ARPES slices in Figure 3 were thus generated by combining slices at incremental $k_\perp$ values for the two orientations indicated in Figure 1, where the colors represent the $k_\perp$ value within the bulk Brillouin zone relative to Γ, showing an intuitive visualization of the emission from empty states. From this simple observation it is shown that upon thermalization into the conduction band, secondary electrons lose their initial valence band state information and hence fully reflect the empty final states. The integration of states through $k_\perp$ also indicates no fundamental selection in $k_\perp$ during emission. This is in stark contrast with conventional ARPES, where $k_\perp$ cutting is observed.[20,21]

Figure 3 shows images acquired using both 21.2 eV (Figure b,e) and 40.8 eV (Figure c,f) excitation, while a broad-spectrum Hg discharge lamp was also used (Figure S1, Supporting Information), all providing consistent data. This not only reaffirms the lack of valence band state dependence within this energy region, but also an independence from the method of secondary electron generation, including the use of primary electron excitation.[14] Using the $k_\perp$-integration model for secondary electron emission, as in Figure 3, ARPES from higher energy state emissions within the conduction band were also compared (Figure S2 and Movie S1b–e, Supporting Information). The model fits well with the ARPES images up to at least 10 eV above the VBM, but the greater number of bands and energy approximations lead to more noticeable discrepancies at higher energies.[15] However, comparison using 21.2 and 40.8 eV excitation shows that emission up to 13 eV above the VBM was still dominated by the conduction band states for both (100) and (111) surfaces (Movie S1b–e, Supporting Information), indicating that a significant portion of unoccupied states can be mapped directly using ARPES of secondary electrons.

This phenomenon is further confirmed on a copper (100) crystal, where secondary electron ARPES was performed from 6 to 10 eV above the Fermi level (E_F). As a metal, copper lacks the CBM and NEA present in diamond and the secondary electron intensity is therefore significantly weaker. Nonetheless, part of the copper unoccupied states was observed and compared with the calculated bands in **Figure 4**a using (b) 21.2 and (c) 40.8 eV excitation energy (further elaboration on this crystal is presented in Figure S3, Supporting Information). The sharp features in Figure 4b can also be used to determine the momentum resolution of our methods. We found Δk to be 0.05 Å^{-1}, close to the regular ARPES resolution (0.03 Å^{-1}) determined using the Fermi surface. These unoccupied band features explain the atypical shoulders seen in the low energy region of the copper UPS spectra (Figure S4, Supporting

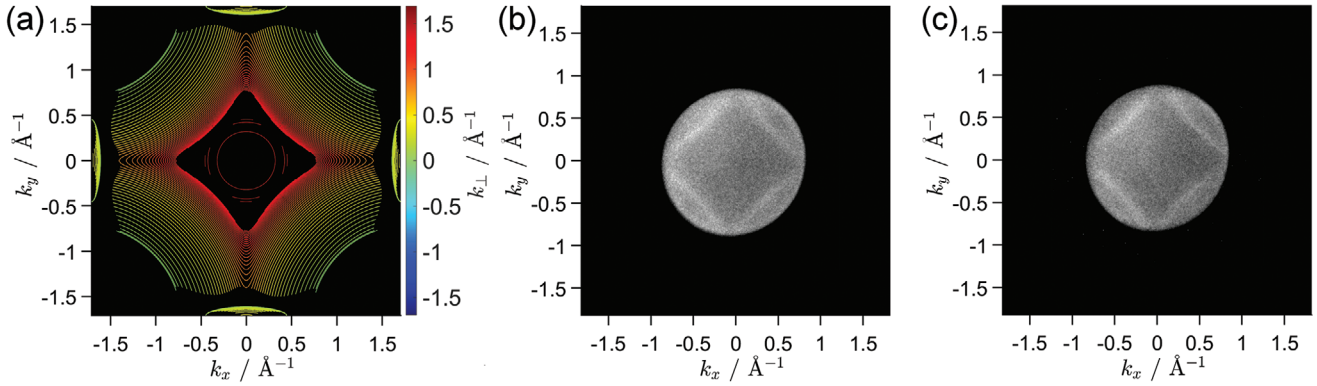

Figure 4. a) Calculated empty states of copper from a 3D bulk band at 7.2 eV above the Fermi level, compared with full-wavevector ARPES image of copper (100) using b) 21.2 eV and c) 40.8 eV photon excitation.

Information). The copper UPS spectra in Figure S4 using two different photon energies are identical up to ≈11 eV, where the onset of the occupied d-bands began for the 21.2 eV illumination. This confirms the applicability of our secondary electron emission models to virtually all crystalline materials.

The measurements performed here use identical methods to those used in conventional ARPES, only in a lower kinetic energy region; as described above though, they have distinctly different emission spectra. To investigate the origins of these differences, we reference the three-step model commonly used to describe standard photoemission kinematics,[21] namely 1) vertical (momentum-less) photoexcitation, 2) electron transport, and 3) electron emission. The secondary electrons measured here underwent an additional process of thermalization between steps (1) and (3), occupying the lower energy empty bands and losing information of initial occupied bands gained in step (1). As was observed from Figure 3, the emission from unoccupied states are $k_\perp$ integrated in contrast to a photon-dependent $k_\perp$ slice selection in conventional ARPES. This indicates that the $k_\perp$ selection typically observed occurs during the photo-absorption and excitation in the bulk in step (1) rather than at the surface in step (3). This selection is done by the momentum matching between the initial occupied states and the free-electron-like final states, which is required for a vertical transition. The onset of these free-electron-like states in materials can easily be found by applying the method described here using different photon energies and comparing the low energy emissions (Figure S2, Supporting Information). This might be of interest from the theoretical perspective and offer insight on required photon energies for standard ARPES experiments. Electron emission from sub-band gap excitation energy can also be used for the study of excitons in the material,[28] where any anisotropies can potentially be studied using ARPES in this region.

Excited electrons decay randomly into empty states within the crystal, indiscriminately regardless of k. The thermalized electrons from the bulk traveling through the surface will feel the potential at the surface and adhere to these bands. This means that any electrons measured in this region will reflect the band dispersion and energy at the surface, offering an extremely high surface sensitivity. It may provide invaluable information when studying surface band bending or heterojunctions. However, the secondary electrons are generated in the bulk through inelastic scattering as they travel to the surface, where the final distribution has a dependence on the depth traveled;[31] this can also explain the different ratios of elastic and inelastic electrons from UPS using different light sources (Figure S4, supporting Information). It should therefore be noted that while the bands measured in the low energy region reflect the states at the surface, the energy distribution can be influenced by the underlying bulk material, depending on its density of states and the excitation energy used.

Energy with respect to a fixed k (green line in Figure 3b) is shown in **Figure 5**, where the CBM and the vacuum level are clearly visible. Direct determination of the NEA of a hydrogen terminated diamond (100) surface is hence allowed, giving a value of –1.0 eV.[25,26] The intense signal near the CBM across $k_\parallel$ suggests inelastic electron–electron scattering during emission, and the uniform emission below the CBM from within the band gap indicates contributions from surface emission, where vacuum free-electron states tail into the surface as evanescent waves and provide a small density of states for electrons to emit from.[14] The non-negligible band gap emission suggests a significant contribution of vacuum states at the surface, which can have implications for electron emission devices and thin film electronics.

An NEA-exhibiting sample orientated such that the CBM lies at $k_\parallel = 0$ allows for direct imaging of the CBM. The energy dispersion within the CBM valley is clearly visible in Figure 5a, outlined in blue dashes. The orange dashed parabola represents the free-electron horizon $k_{\parallel,\max}$ and was fit using Equation (1). Likewise, the valley dispersion (blue) was fit up to 0.7 eV above the CBM, where, due to the proximity to the Brillouin zone boundary, the parabolic approximation of the dispersion relation is no longer valid and a cross forms for both the calculated and experimental bands (Figure 3a–c). The parabola positions were determined using sigmoidal fits on line profiles at each energy (Figure 5b). The curvature ratio between the two parabolas gives the effective mass of electrons in the CBM of diamond in the transverse direction (green dashed lines in Figure 1), m_t, which was found to be $0.21 \pm 0.015\ m_e$.

Our experimentally determined m_t agrees well with first principles calculations of $0.22\ m_e$ from Löfås et al.[32] Provided that a larger NEA is possible, the longitudinal electron mass (orange dashed lines, Figure 1) would also be obtainable through the (100) surface using the valleys on the $k_\perp = 0$ plane.

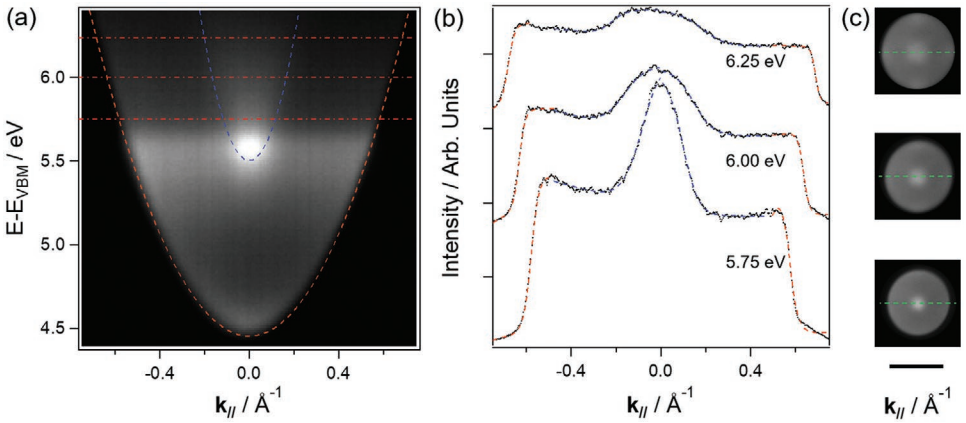

Figure 5. a) ARPES of the diamond (100) surface near the CBM, where $k_{\parallel}$ is a cut in k through energy in the $X-\Gamma-X$ direction. The parabolas represent the free-electron dispersion (orange), and the dispersion near the CBM of diamond (blue). The red horizontal lines are the selected energies for the b) line profiles and c) full-wavevector ARPES. b,c) Line profiles and full-wavevector ARPES images extracted at 5.75, 6.00 and 6.25 eV. b) Dotted orange and blue lines represent the sigmoid fitting of the free-electron parabola and CBM, respectively. c) The green dotted lines represent the k-space cutting used in (a).

This method is feasible owing to the integrated signal along $k_{\perp}$ during secondary electron emission, meaning all states are sampled without a preferential $k_{\perp}$ value. This demonstrates a novel yet simple technique to directly obtain electron effective masses in conduction band valleys, while effective mass has traditionally been difficult to obtain experimentally.

3. Conclusion

In conclusion, we have used secondary electron ARPES to directly observe the conduction band of diamond up to 13 eV above the VBM and the empty states of copper up to 9 eV above the Fermi level. These matched well with our theoretical model for electron emission from bulk states. With this, we have shown that in this mode of emission there is no selection in $k_{\perp}$ but electrons still respect $k_{\parallel}$ and energy conservation rules. In some cases, for example semiconductors, these analyses can be exploited to extract vital information about empty states (e.g., the electron mass at the CBM) which are generally overlooked in ARPES investigations. More generally, we confirm the findings of Bovet et al.[24] showing a simple way of directly observing unoccupied electronic states while retaining the energy and momentum resolution to conventional ARPES. We proved the method applicability on different materials, the independence from the incoming photon energy and demonstrated the effectiveness of the PEEM full-wavevector images. We envisage these new findings provide useful insights on the exploration of material properties using the low energy secondary electron emission process. For the material characterization community, we show that empty-state information is obtainable with a relatively simple photoemission experiment.

4. Experimental Section

Computational: The diamond band structure was calculated using density functional theory (DFT) in Cambridge serial total energy package (CASTEP).[33] A two-atom primitive unit cell was used for the bulk diamond structure. The Perdew–Burke–Ernzerhof solids (PBEsol)[34] generalized gradient approximation (GGA) provided the exchange-correlation potential and plane-waves up to an energy of 900 eV constructed the electron density. A Monkhorst–Pack (MP)[35] grid of $20 \times 20 \times 20$ special k-points sampled the Brillouin zone. The band gap was increased to 5.47 eV[27] post-calculation due to its well-documented underestimation by the GGA functional.[34] Likewise, the copper was calculated using the same procedure but with a single atom unit cell.

An $81 \times 81 \times 47$ grid of k-points was input into the CASTEP band calculation to generate a 3D band structure within the first Brillouin zone, which could then be rotated to represent specific crystal orientations, that is, diamond (100) and (111).

Experimental: (100) and (111) orientated diamond substrates purchased from Element Six and Euro Superabrasives, respectively, were cleaned in a fuming sulfuric and nitric acid mixture for 3 h, then capped with a conductive boron doped diamond using an ASTeX type microwave plasma reactor. Capping layers were grown for 10 min with 3 % methane in hydrogen, with an additional 100 ppm of B_2H_6 in methane, at about 850 °C substrate temperature. Hydrogen termination was then done in a pure hydrogen plasma at 500 °C. Copper (100) was purchased from MaTeK and used as received.

Samples were cleaned and analyzed at the Bristol NanoESCA Facility under ultra-high vacuum (UHV) conditions. Diamond was cleaned by UHV annealing at 300 °C, while copper (100) was cycled through a series of alternating sputtering at 0.5 keV of Ar and annealing at 600 °C.

Full-wavevector ARPES was performed using a double hemispherical analyzer energy-filtered k-photoemission electron microscopy (PEEM) at room temperature, with an overall temperature-limited energy resolution of ≈100 meV at the Fermi edge and work function cut-off of copper. The light sources included monochromated He-I and He-II emission ($h\nu = 21.2$ and 40.8 eV), and a broad-spectrum Hg lamp ($h\nu < 5.8$ eV).

Supporting Information

Supporting Information is available from the Wiley Online Library or from the author.

Acknowledgements

Experiments were carried out at the Bristol NanoESCA Facility partially under the EPSRC Strategic Equipment Grant EP/K035746/1

and EP/M000605/1. The authors thank M. Williams for advice and useful discussion on DFT calculations. G.W. acknowledges funding for the Ph.D. studentship through BCFN: Renewtec Technologies, Al Hamad Group.

Conflict of Interest

The authors declare no conflict of interest.

Keywords

angle-resolved photoemission spectroscopy, band structure, effective mass, secondary electrons, unoccupied states

Received: August 27, 2020
Revised: October 1, 2020
Published online: October 15, 2020

[1] M. J. Stern, L. P. René de Cotret, M. R. Otto, R. P. Chatelain, J.-P. Boisvert, M. Sutton, B. J. Siwick, *Phys. Rev. B* **2018**, *97*, 165416.
[2] S. Ulstrup, A. G. Čabo, J. A. Miwa, J. M. Riley, S. S. Grønborg, J. C. Johannsen, C. Cacho, O. Alexander, R. T. Chapman, E. Springate, M. Bianchi, M. Dendzik, J. V. Lauritsen, P. D. C. King, P. Hofmann, *ACS Nano* **2016**, *10*, 6315.
[3] A. Lanzara, P. V. Bogdanov, X. J. Zhou, S. A. Kellar, D. L. Feng, E. D. Lu, T. Yoshida, H. Eisaki, A. Fujimori, K. Kishio, J.-I. Shimoyama, T. Noda, S. Uchida, Z. Hussain, Z.-X. Shen, *Nature* **2001**, *412*, 510.
[4] G. D. Scholes, G. Rumbles, *Nat. Mater.* **2006**, *5*, 683.
[5] S.-H. Ji, T. Zhang, Y.-S. Fu, X. Chen, X.-C. Ma, J. Li, W.-H. Duan, J.-F. Jia, Q.-K. Xue, *Phys. Rev. Lett.* **2008**, *100*, 226801.
[6] J. B. Pendry, *J. Phys. C Solid State Phys.* **1981**, *14*, 1381.
[7] A. Goldmann, M. Donath, W. Altmann, V. Dose, *Phys. Rev. B* **1985**, *32*, 837.
[8] E. Fortunato, P. Barquinha, R. Martins, *Adv. Mater.* **2012**, *24*, 2945.
[9] R. Fiederling, M. Keim, G. Reuscher, W. Ossau, G. Schmidt, A. Waag, L. W. Molenkamp, *Nature* **1999**, *402*, 787.
[10] J. Isberg, M. Gabrysch, J. Hammersberg, S. Majdi, K. K. Kovi, D. J. Twitchen, *Nat. Mater.* **2013**, *12*, 760.
[11] R. Jansen, *Nat. Mater.* **2012**, *11*, 400.
[12] J. W. Schwede, I. Bargatin, D. C. Riley, B. E. Hardin, S. J. Rosenthal, Y. Sun, F. Schmitt, P. Pianetta, R. T. Howe, Z.-X. Shen, N. A. Melosh, *Nat. Mater.* **2010**, *9*, 762.
[13] B. C. Stipe, M. A. Rezaei, W. Ho, *Rev. Sci. Instrum.* **1999**, *70*, 137.
[14] R. F. Willis, N. E. Christensen, *Phys. Rev. B* **1978**, *18*, 5140.
[15] V. N. Strocov, R. Claessen, G. Nicolay, S. Hüfner, A. Kimura, A. Harasawa, S. Shin, A. Kakizaki, P. O. Nilsson, H. I. Starnberg, P. Blaha, *Phys. Rev. Lett.* **1998**, *81*, 4943.
[16] M. W. Rowe, H. Liu, G. P. Williams, R. T. Williams, *Phys. Rev. B* **1993**, *47*, 2048.
[17] B. Lv, T. Qian, H. Ding, *Nat. Rev. Phys.* **2019**, *1*, 609.
[18] A. Locatelli, T. O. Menteş, M. Á. Niño, E. Bauer, *Ultramicroscopy* **2011**, *111*, 1447.
[19] J. T. Grant, *Surf. Interface Anal.* **1989**, *14*, 271.
[20] F. Himpsel, *Adv. Phys.* **1983**, *32*, 1.
[21] A. Damascelli, *Phys. Scr.* **2004**, *T109*, 61.
[22] S. L. Molodtsov, A. Puschmann, C. Laubschat, G. Kaindl, V. K. Adamchuk, *Phys. Rev. B* **1991**, *44*, 1333.
[23] S. L. Molodtsov, C. Laubschat, G. Kaindl, V. K. Adamchuk, *Phys. Rev. B* **1992**, *46*, 12802.
[24] M. Bovet, V. N. Strocov, F. Clerc, C. Koitzsch, D. Naumović, P. Aebi, *Phys. Rev. Lett.* **2004**, *93*, 107601.
[25] L. Diederich, P. Aebi, O. Küttel, L. Schlapbach, *Surf. Sci.* **1999**, *424*, L314.
[26] J. Cui, R. Graupner, J. Ristein, L. Ley, *Diam. Relat. Mater.* **1999**, *8*, 748.
[27] P. J. Dean, E. C. Lightowlers, D. R. Wight, *Phys. Rev.* **1965**, *140*, A352.
[28] C. Bandis, B. B. Pate, *Phys. Rev. B* **1995**, *52*, 12056.
[29] P. Baumann, R. Nemanich, *Surf. Sci.* **1998**, *409*, 320.
[30] G. Wan, M. Cattelan, N. A. Fox, *J. Phys. Chem. C* **2019**, *123*, 4168.
[31] J. Scholtz, D. Dijkkamp, R. Schmitz, *Philips J. Res.* **1996**, *50*, 375.
[32] H. Löfas, A. Grigoriev, J. Isberg, R. Ahuja, *AIP Adv.* **2011**, *1*, 032139.
[33] S. J. Clark, M. D. Segall, C. J. Pickard, P. J. Hasnip, M. I. J. Probert, K. Refson, M. C. Payne, *Zeitschrift für Krist. - Cryst. Mater.* **2005**, *220*, 567.
[34] J. P. Perdew, A. Ruzsinszky, G. I. Csonka, O. A. Vydrov, G. E. Scuseria, L. A. Constantin, X. Zhou, K. Burke, *Phys. Rev. Lett.* **2008**, *100*, 136406.
[35] J. D. Pack, H. J. Monkhorst, *Phys. Rev. B* **1977**, *16*, 1748.

